Supplemental Information on Methods:

Genotyping

Genomic DNA was obtained from tail biopsies according to standard protocols and genotyping was performed by PCR using the following primers: Oatp1c1 fwd: 5'-CACTGCCCTGTCCTGTAGGT-3' and Oatp1c1 rev: 5'-CATCGCTTGATG-AGTGGTCTTG-3' were used with an annealing temperature of 58 °C in order to discriminate between wt and fl alleles with expected sizes of 693 bp and 787 bp respectively as well as Oatp1c1 del rev: 5'-ACCATGTGGTTGTTGGGAAT-3' to detect the delta allele indicated by a 551 bp product. Mct8 fwd: 5'-TGTGAGTATATTCACTGACCGTTTG-3' in combination with Mct8 rev: 5'-CAATTCAAT-GGTCAAAGCAGGACTG-3' was utilized with an annealing temperature of 60 °C to detect the wt allele with an expected size of 383 bp and together with Mct8 lacZ: 5'-GGGCCAGCTCATTCCTCCCACTCA -3' to visualize the targeted allele (600 bp). Pax8 genotyping was performed at 59 °C. Pax8-1: 5'-GGATGTGGAATGTGTGCGAGG-3', Pax8-2 5'-GCTAAGAGAAGGTGGATGAGA-3' and Pax8-3 5'-GATGCTGCCAGTCTCGTA-3' were used to differentiate the wt allele of 390 bp and the ko allele of 370 bp of size.

Quantitative real-time PCR

The following primers were chosen to generate the PCR fragments: Aldh1a1 5'-AAAATGTCTCCATCACTTGG-3' and 5'-AAGTCTTTGCCAATGCATAC-3'; Crym: 5'-GTCCAGGCGTACAGTCACTA-3' and 5'-AGCCTCCTGCACTGATGAAC-3' CycD: 5'-GCAAGGATGGCA-AGGATTGA-3' and 5'- AGCAATTCTGCCT-GGATAGC-3'; D1: 5'-CGTGACTCCTGAAGATGATG-3' and 5'-CCAATGCCTA-TGGTTCCTAC-3'; D2: TTCCCATTATCTACCTGCTG-3' and 5'-GAACTCCTG-TCAGCATAATG-3';

GPD2: 5'-GGCAGAAGATACCGTGAATG-3' and 5'-CTGGACAAGCCTGATGTAGA-3'; Hr: 5´-AAGCTAAATAGGGGATCCTG-3´and 5´-ATTTGTAGAACGGACCACAC-3´; RC3: 5'-CGACGATATTCTTGACATCC-3' and 5'-CACACTC-TCCGCTCTTTATC. The annealing temperature was 55°C for all primer pairs.

Quantification

For quantifying the results obtained by ISH and immunofluorescence, the respective signal intensities were measured with the open source program ImageJ (NIH). TRH-specific antisense hybridization signals were quantified by encircling the area of the paraventricular hypothalamic nucleus and measuring the area as well as the integrated density in 6-8 brain sections per animal and 4 animals per genotype. Using one sense control per animal, the background ISH signal intensity was assessed and the mean background value over all control sections was estimated. ISH background intensities were extrapolated for the areas measured using antisense cRNA probes and subtracted from the detected integrated densities. In the same way, GHRH signal intensities in the hypothalamic arcuate nucleus as well as integrated ISH densities for SST in the hypothalamic periventricular nucleus were measured. Pituitary GH, D2 and TSH expression was assessed by determining the integrated signal densities in 4 sections per animals using 4 mice per genotype and time point. Hepatic Igf1 expression was quantified in a 300-by-300-µm frame. 4 sections per animal and 4 animals per genotype and time point were used. Wt expression levels were considered as 1. In graphs depicting the results obtained at different time points, wt values at P6 were employed for normalization.

Cerebellar Purkinje cell dimensions which reflect the thickness of the molecular layer were measured at the primary fissure between anterior and posterior cerebellar lobe in calbindin-stained sections. Four consecutive, sagittal sections from each animal (3 per genotype and time point) were subjected to quantification with ImageJ and the

results were normalized to the respective value obtained by analyzing sections from wt animals.

The integrated density of MBP in all areas of the cerebral cortex as well as of FluoroMyelin in the corpus callosum was assessed from bregma level +0.25 to -0.15 mm by ImageJ analysis. Every second section (with four sections per animal) was used for determining either MBP immunoreactivity or FluoroMyelin staining, respectively. Wt values at each time point were considered as 1.

Parvalbumin immunoreactivity was investigated in the barrel field of the somatosensory cortex from bregma level -0.70 to -1.20 mm by staining every second section (with six sections per animal). In an area delimited by the pial surface, the corpus callosum as well as the disappearance of the barrels as anatomical boundaries, the number of PV-positive neurons was counted. Thereby, increasing numbers of PV-positive cells were detected with age ranging from 247±46 cells in wt and zero cells in M/O dko mice at P12 to 570±32 cells in wt and 226±46 cells in M/O dko mice at P120. Values were divided by the dimension of the analyzed area that varied between 1.6 and 2.0 mm^2. In the same manner, the number of calretinin-positive neurons was estimated in the barrel field of the somatosensory cortex by employing four consecutive sections from bregma level -1.30 to -1.50 mm. In a comparable area size as used above, 269±49 CR-positive cells in wt and 369±39 cells in M/O dko mice at P12 and 179±23 cells in wt and 236±28 cells in M/O dko mice at P120 were counted and normalized to the area dimensions.

The relative integrated density of GAD67 and calbindin immunoreactivity was also assessed in the barrel field of the somatosensory cortex between bregma level -0.90 and -1.10 mm using the anatomical boundaries described above. After staining every second section for both markers, the overall integrated density was measured and

normalized to the area proportions. Wt values at each time point were considered as 1.

The thickness of the inner layers of the cerebral cortex (layers V and IV) as well as of the outer layers (I, II/III and IV) was evaluated on images of NeuN immunostained sections in the somatosensory cortex between bregma level -0.55 and -0.75 mm (every second section stained for NeuN, three sections per animal). Originating at the corpus callosum, a line was drawn in a right angle to the pial surface at three different places within the barrel field to measure the overall thickness of the cortex. Likewise, additional lines were drawn at the same positions starting from the corpus callosum to the border of layer IV as defined in Supplemantal Figure 5B to measure the dimension of the inner layers followed by the calculation of the thickness of the outer layers.

In all histomorphological studies, 3 animals per genotype and time point were used and subjected to quantification with ImageJ.

Paraffin sections subjected to Bielschowsky's as well as Gallyas' silver impregnation were quantified by measuring the thickness of the corpus callosum between bregma level +0.50 and +0.10 mm by using ImageJ analysis software. Four sections per animal were analyzed using at least three mice per genotype and time point.

Ultrathin sectioning and electron microscopy

For EM-studies animals at P21 were anaesthetized with isoflurane and perfused intracardially with 15 ml cold HBSS containing 7.5 mM EDTA, followed by 20 ml of freshly prepared cold fixative (2.5% glutaraldehyde, 4% paraformaldehyde in PBS). Brains were removed and postfixed for at least two days. Brains were cut with a vibratome. Brain tissue containing the corpus callosum between the midline and the cingulum bundle was isolated, then postfixed with OsO_4, dehydrated and embedded

in Epon. Ultrathin sections (50 nm) were produced using an Ultracut S microtom (Leica) and electron micrographs were taken on a JEM 1400 electron microscope (JEOL) using an accelerating voltage of 80 kV and coupled with Orius SC 1000 CCD-camera (GATAN).

Gait analysis

At least 6 male mice per group at the age of 5 months were trained to run on a piece of filter paper. At the day of testing, nontoxic ink was applied to the hind paws, and each animal was forced to walk 3 times. Footprint traces were analyzed with regard to the stride length and the hind paw angle.

Rotarod test

Motor-coordination activity was tested utilizing an accelerating rotarod (TSE Systems). For the analysis depicted in Figure 8C, 4 month- old male and female mice (5-7 per genotype and gender) were familiarized to the system by allowing them to run once on the rotating rod with a constant velocity of 5 rpm. On the following day, the settings were changed to an acceleration of the rod rotation from 5-50 rpm within the maximum testing period of 300 seconds. The animals were analyzed for 5 consecutive days with 2 trials per day and the time the mice remained on the roller was monitored and averaged.

Beam walk test

Beam walk testing was performed following protocols described by (55). Male mice at the age of five months (6-8 per genotype) were forced to cross an elevated beam of 100 cm length and 1 cm width 3 times per day for 3 consecutive days in order to become acquainted to the task. On the following 4 days, the trials were recorded for calculating the total number of hind limb slips per run and the time period needed to cross the beam.

Hanging wire test/Grip strength meter

To unravel neuromuscular abnormalities, four months old male and female mice (5-7 per genotype and gender) were placed onto a metal wire that was then turned upside down. Animals were monitored for their capacity to cling to the wire for a maximal period of 60 sec, and the time period until the mice fell down was recorded. Each animal was tested 3 times per day on 3 consecutive days. To evaluate muscle strength and neuromuscular functioning, fore limp grip strength was measured with a high-precision force sensor (TSE Systems) according to the manufacturer´s instruction using eight female mice of each genotype at the age of one year. Recording was repeated six times per animal.

Suppl. Fig. 1

A

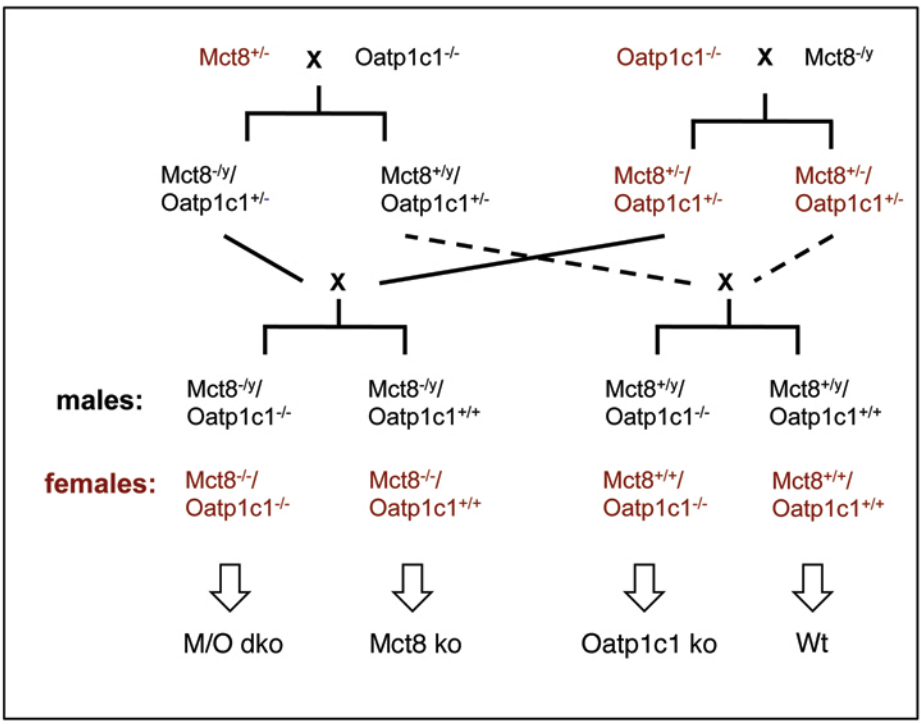

B

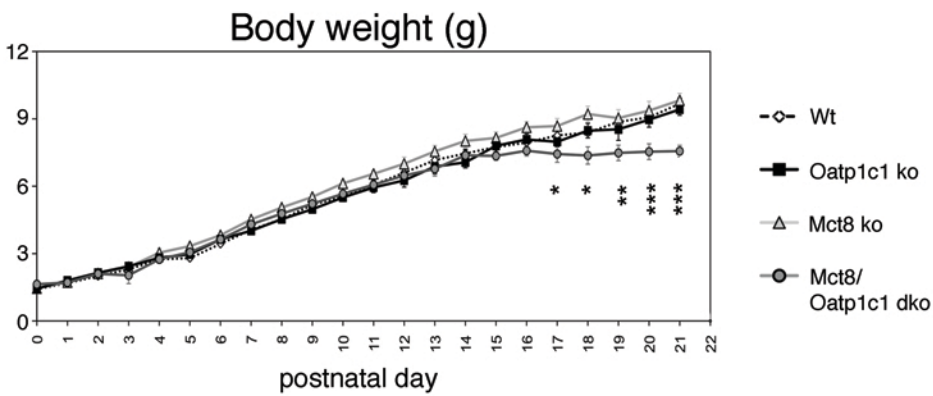

C

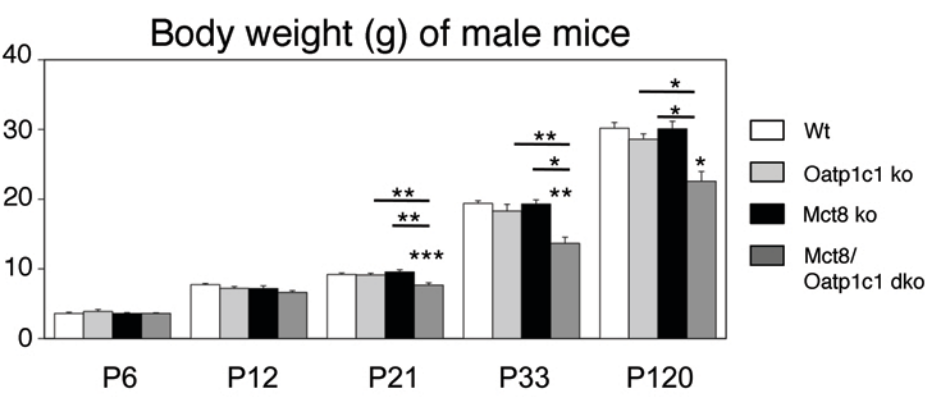

Suppl. Fig. 2

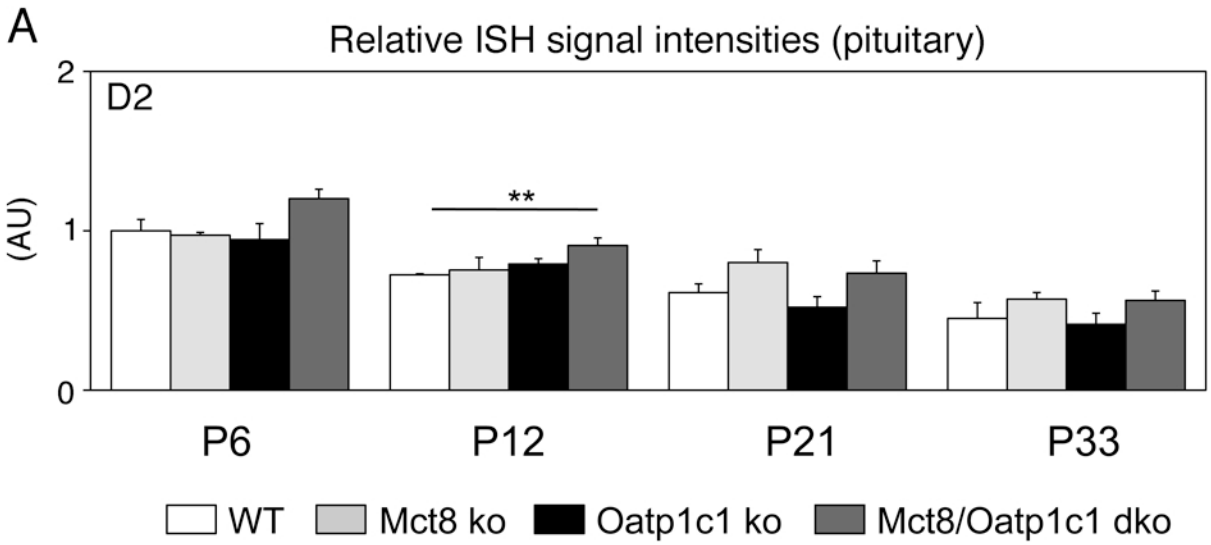
A
Relative ISH signal intensities (pituitary)
D2
(AU)
2
1
0
**
P6
P12
P21
P33
WT
Mct8 ko
Oatp1c1 ko
Mct8/Oatp1c1 dko

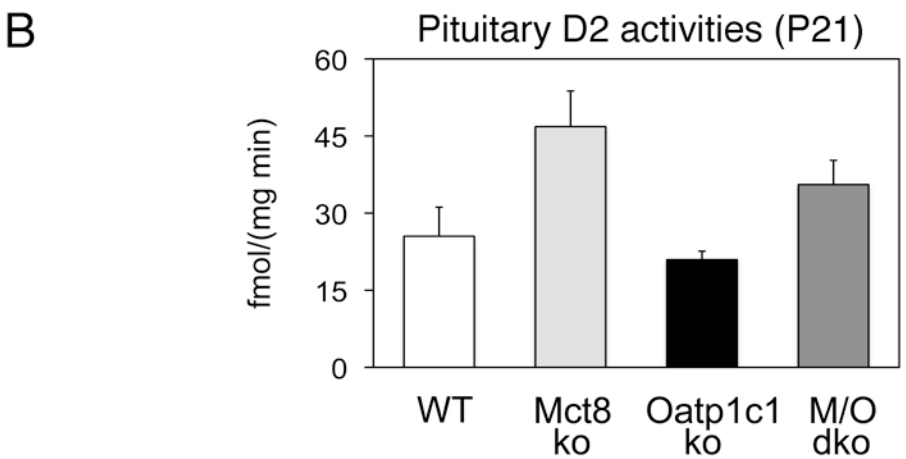
B
Pituitary D2 activities (P21)
fmol/(mg min)
60
45
30
15
0
WT
Mct8 ko
Oatp1c1 ko
M/O dko

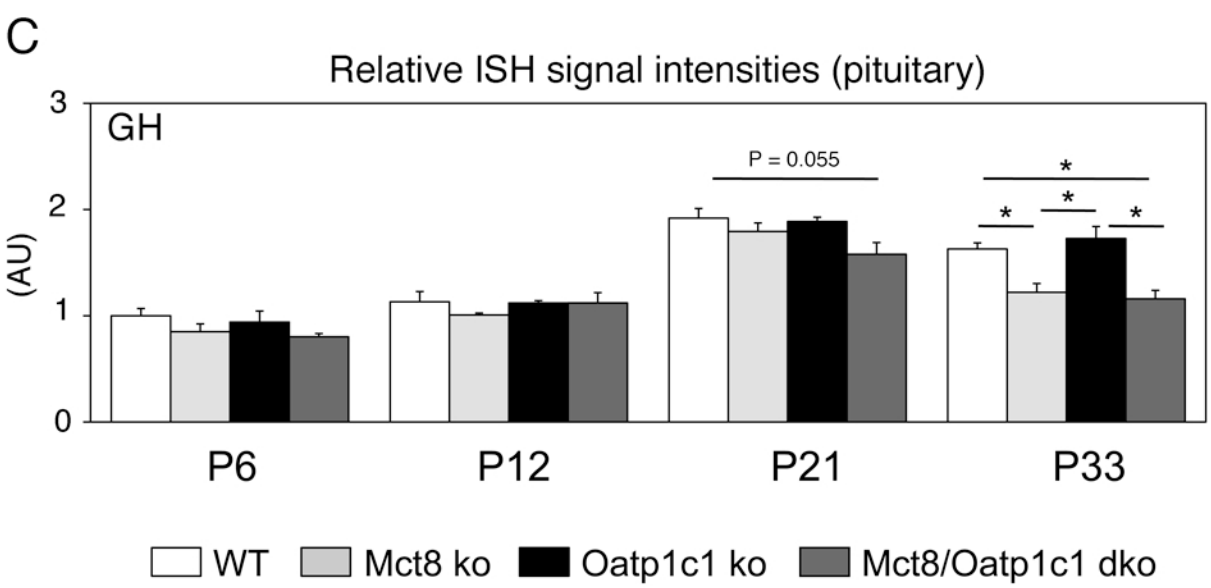
C
Relative ISH signal intensities (pituitary)
GH
(AU)
3
2
1
0
P = 0.055
*
*
*
*
P6
P12
P21
P33
WT
Mct8 ko
Oatp1c1 ko
Mct8/Oatp1c1 dko

Suppl. Fig. 3

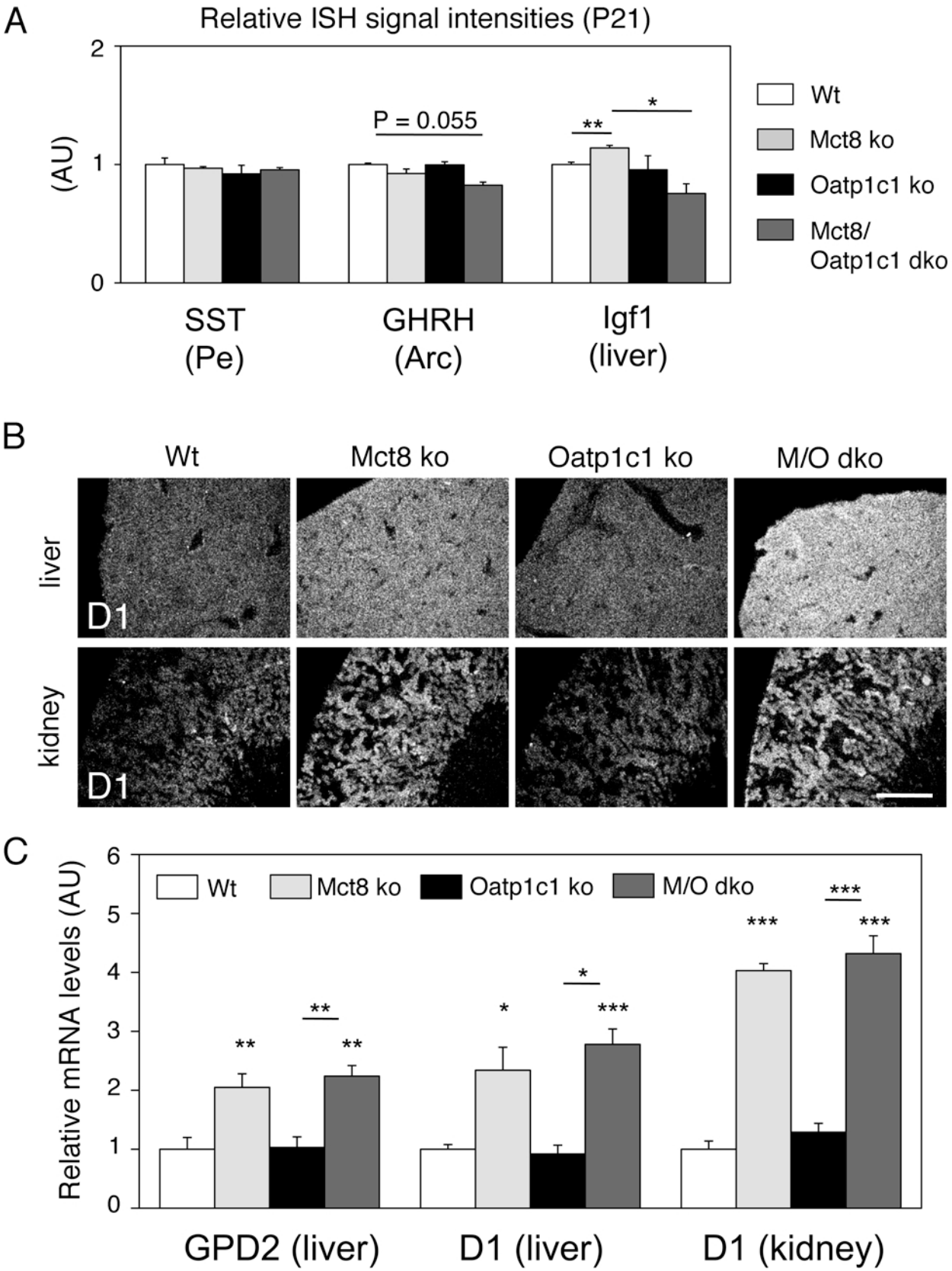
A
Relative ISH signal intensities (P21)
(AU)
2
1
0
P = 0.055
**
*
Wt
Mct8 ko
Oatp1c1 ko
Mct8/
Oatp1c1 dko
SST
(Pe)
GHRH
(Arc)
Igf1
(liver)
B
Wt
Mct8 ko
Oatp1c1 ko
M/O dko
liver
kidney
D1
D1
C
Relative mRNA levels (AU)
6
5
4
3
2
1
0
Wt
Mct8 ko
Oatp1c1 ko
M/O dko
**
**
**
*
*
***
***
***
***
GPD2 (liver)
D1 (liver)
D1 (kidney)

Suppl. Fig. 4

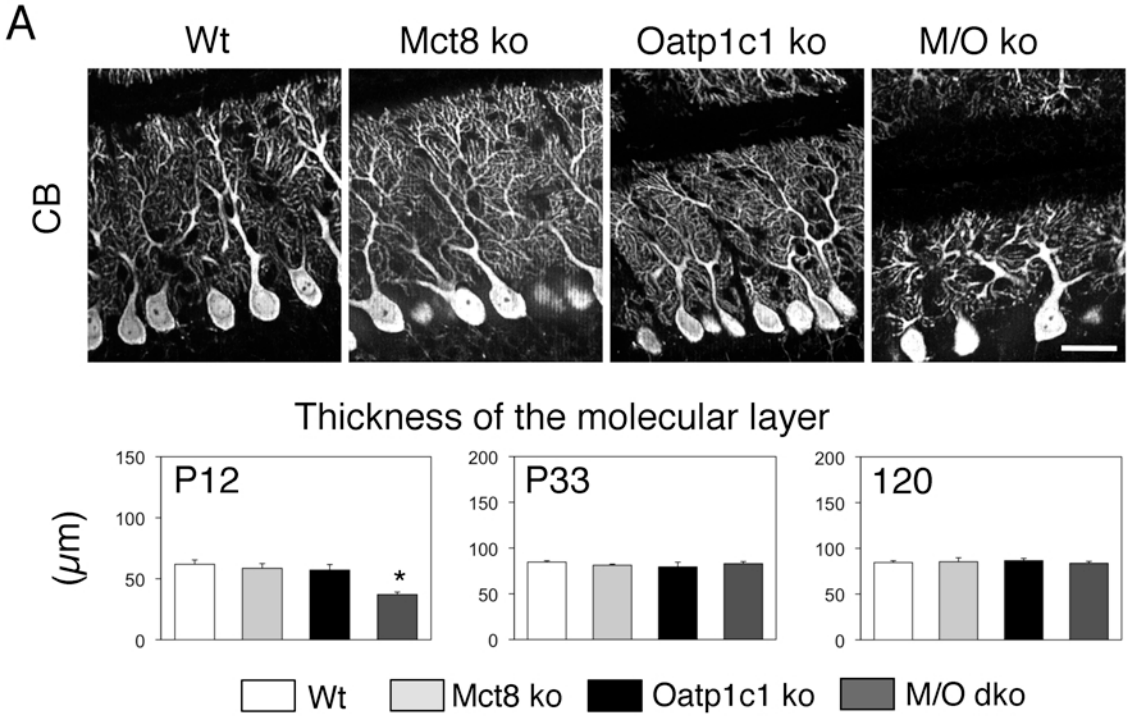
A
Wt
Mct8 ko
Oatp1c1 ko
M/O ko
CB
Thickness of the molecular layer
(μm)
P12
P33
120
150
100
50
0
200
150
100
50
0
*
Wt
Mct8 ko
Oatp1c1 ko
M/O dko

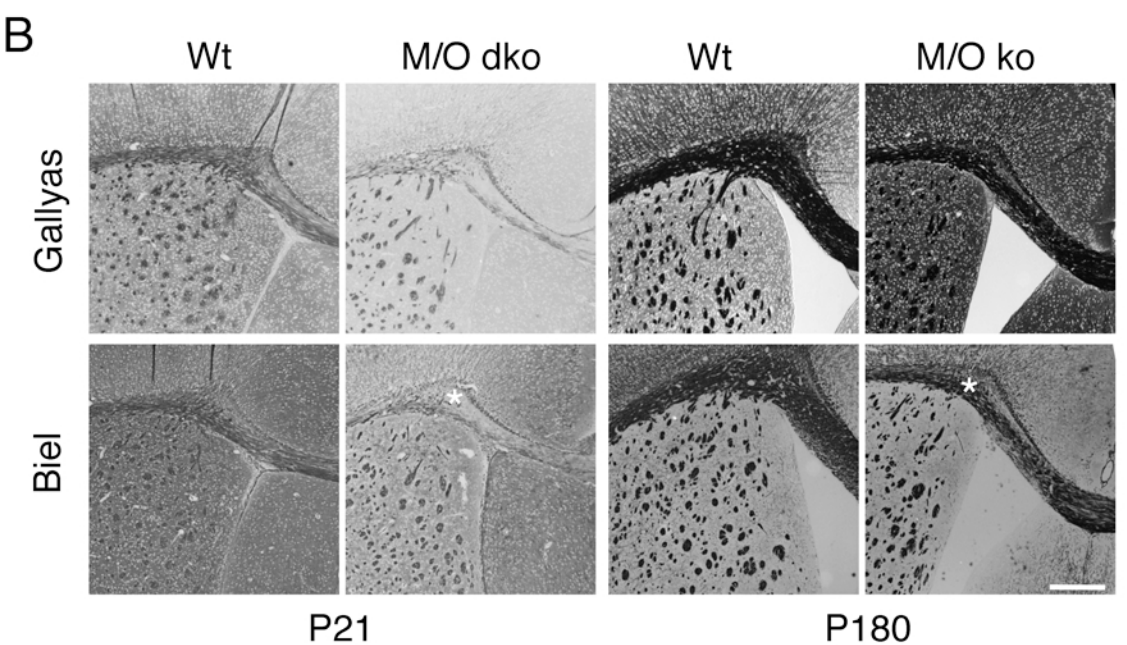
B
Wt
M/O dko
Wt
M/O ko
Gallyas
Biel
*
*
P21
P180

Suppl. Fig. 5

A

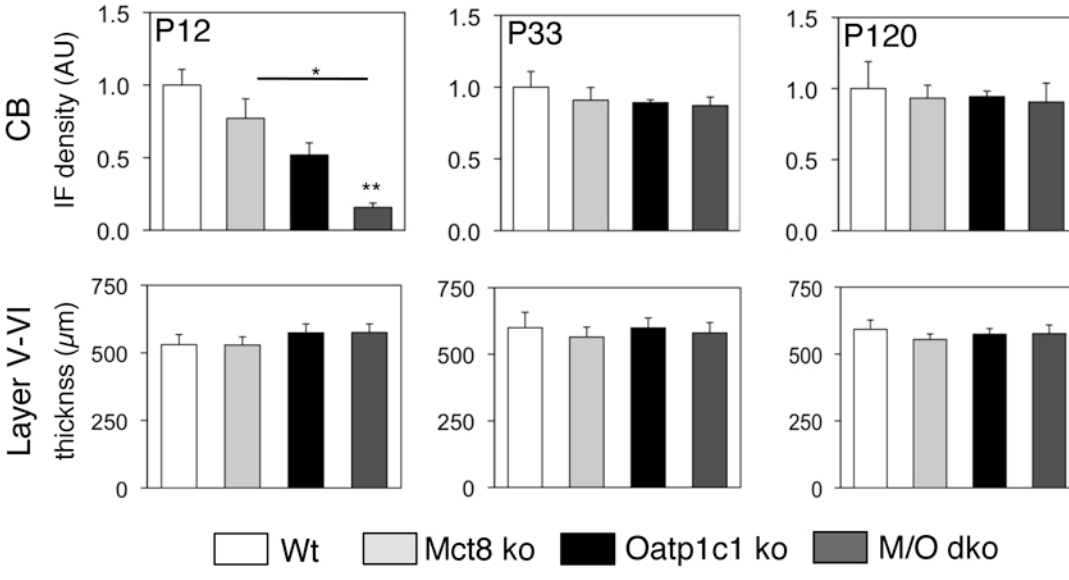

B

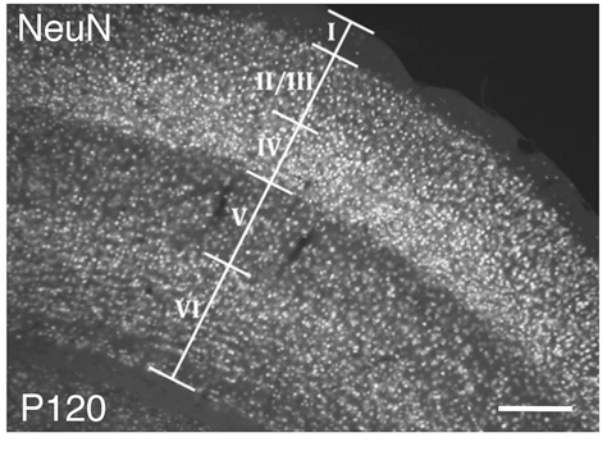

Suppl. Fig. 6

A

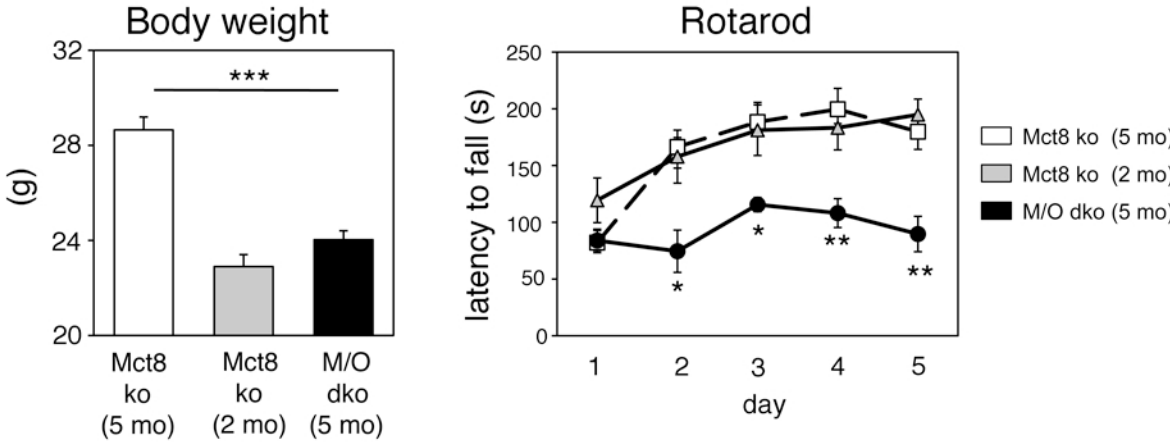

B

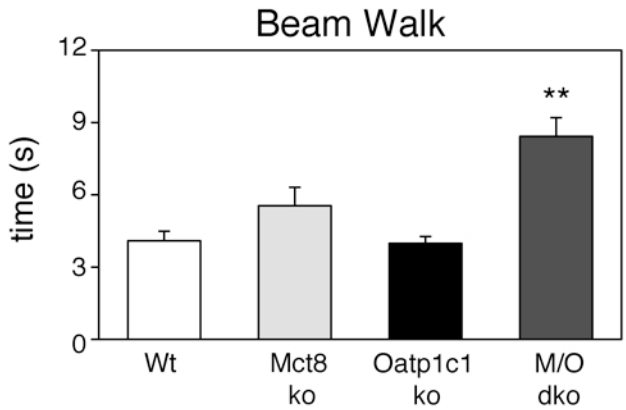

Supplemental Figure 1: Breeding strategy and growth curve (A) Schematic illustration of the breeding strategy to produce male (black color) and female (red color) TH transporter mutant animals. Due to the location of the *Mct8* gene on the X-chromosome, male mice are either wild type ($Mct8^{+/y}$) or deficient ($Mct8^{-/y}$) for Mct8. (B). Following the generation of Mct8/Oatp1c1 dko mice body weight of the animals (n = 8-12 per genotype from 16 litters with a litter size of 5-8 pups) was recorded daily within the first three postnatal weeks. Starting from postnatal day 17, Mct8/Oatp1c1 dko mice gained significantly less weight than wild type, Mct8 ko and Oatp1c1 ko littermates. (C) Body weight of all male animals used for the described experiments were monitored and revealed a significant reduction in Mct8/Oatp1c1 dko mice at the age of P21 and older (n=7-21 per genotype). *P<0.05, **P<0.01, ***P<0.001.

Supplemental Figure 2: Analysis of pituitary D2 and GH expression (A) Pituitary D2 expression was analyzed by ISH (n=4 per genotype and time point) and revealed increased transcript levels in Mct8/Oatp1c1 dko mice at P6 and P12 whereas at later

time points, no differences between Mct8 ko and Mct8/Oatp1c1 dko mice could be noted. (B) Similar results were obtained by determination of D2 activities in pituitary homogenates at P21. (C) Pituitary GH expression was examined by ISH as well. Whereas at P6 and P12 no differences between the genotypes could be noted, Mct8/Oatp1c1 dko mice showed a slight decrease in GH mRNA expression at P21. *P<0.05, **P<0.01.

Supplemental Figure 3: Examination of the somatotropic axis and thyroidal state of liver and kidney. (A) Expression of central components of the somatropic axis as well as of the GH-downstream mediator Igf1 was analyzed by ISH at P21, and signal intensities were quantified using ImageJ (n=3). Whereas somatostatin (SST) expression in the hypothalamic periventricular nucleus (Pe) was unaltered, GHRH mRNA levels were slightly reduced in the hypothalamic arcuate nucleus (Arc) of Mct8/Oatp1c1 dko animals. Hepatic Igf1 expression was marginally increased in Mct8 ko mice but significantly reduced upon inactivation of both TH transporters. For determining the hepatic and renal thyroidal state, type 1 deiodinase (D1) expression was evaluated in liver and kidney sections from animals (n=4 per genotype) at P21 by ISH (B) and qPCR analysis (C). In both experiments, similarly elevated D1 transcript levels were found in Mct8 ko and Mct8/Oatp1c1 dko mice. In addition, hepatic α glycerol-3-phosphate dehydrogenase (GPD2) expression was assessed by qPCR and revealed increased levels in Mct8 ko and Mct8/Oap1c1 dko as well. *P<0.05, **P<0.01, ***P<0.001.

Supplemental Figure 4: Mct8/Oatp1c1 dko mice display a retarded cerebellar development and reduced myelination: (A) Cerebellar Purkinje cell (PC) morphology in sagittal vibratome sections (n=3 per genotype and time point) was

visualized by calbindin immunofluorescence staining and revealed a poorly developed dendritic tree in Mct8/Oatp1c1 dko mice at P12 (upper layer). Quantification of the thickness of the molecular layer (ML) that reflects PC dendrite dimensions confirmed the optical impression at P12. However, at P33 and P120, the differences in the ML thickness disappeared. Scale bar: 25 µm. (B) Paraffin-embedded forebrain sections were subjected to Gallyas and Bielschowsky (Biel) silver impregnation (n=3-4 per genotype and time point). In both stainings the thickness of the corpus callosum measured at the cingulum bundle (asterisks) is visibly reduced in Mct8/Oatp1c1 double mutant mice at P21 and P180. Scale bar: 500 µm.

Supplemental Figure 5: Consequences of Mct8/Oatp1c1 deficiency on brain morphology and locomotor function. (A) In addition to the data depicted in Figure 7, histomorphological analysis of the somatosensory cortex also included the examination and quantification of frontal brain sections stained with an antibody against the calcium binding protein calbindin (CB). Determination of the integrated immunofluorescence signal densities revealed a significant reduction at P12 in Mct8/Oatp1c1 dko mice but no differences at later time points. NeuN-stained sections were employed to determine the thickness of the deeper cortical layers V-VI but did not reveal any differences. *P<0.05. (B) Illustration of the different cortical layers in NeuN immunostained coronal brain sections at P120. Scale bar: 250 µm.

Supplemental Figure 6: Rotarod and Beam walk test (A) A second cohort of male animals consisting of 5 month-old Mct8 ko and Mct8/Oatp1c1 dko mice as well as 2 month-old Mct8 ko mice (n=4-7 per genotype) was subjected to Rotarod test as described in Figure 8C. Again, Mct8/Oatp1c1 dko mice showed a poor performance

compared to Mct8 ko mice of either the same age or the same body weight. (B) Beam-walk tests were performed as shown in Figure 8D. Mct8/Oatp1c1 dko mice did not only display an increased number of hind limp slips but also needed a significantly longer time to cross the beam compared to the single mutant and wild type animals. *P<0.05, **P<0.01 ***P<0.001.